SYMCOMP 2015
Faro, March 26-27, 2015

SECOND-ORDER FINITE VOLUME MOOD METHOD FOR THE SHALLOW WATER WITH DRY/WET INTERFACE

Jorge Figueiredo[1*], Stéphane Clain[1,2]

1: Centre of Mathematics
School of Sciences
University of Minho
Campus de Azurém, 4800-058 Guimarães, Portugal
e-mail: {jmfiguei,clain}@math.uminho.pt

2: Institut de Mathématiques de Toulouse
Université Paul Sabatier
31062 Toulouse, France

Keywords: finite volume, dry/wet interface, shallow water equation, hydrostatic reconstruction

Abstract. *The shallow water system is a fundamental work-piece for tsunami or flooding simulations. One of the major difficulties is the correct location of the dry/wet interface to evaluate accurate approximations of the velocity and kinetic energy. On the other hand, the MOOD method has been recently proposed to provide more efficient schemes in the framework of the Euler system. We propose to compare two second-order methods, namely the MUSCL and the MOOD techniques, and draw comparisons on accuracy shock capturing and dry/wet interface.*

1 INTRODUCTION

Shallow water equations with varying bathymetry is a challenging topic due to the wide number of applications such that tsunami, flooding, coastal erosion [14]. A large number of numerical schemes has been proposed and studied and, in particular, very high-order finite volume methods (fifth- and sixth-order for instance) have received great attention in order to provide very accurate numerical solutions [10, 11, 7]. Nevertheless, the design of new second-order methods is still an important objective since most of the engineering or environmental applications are developed with such a technique due to its simplicity and computational efficiency [1, 9, 15]. Recently, a new limiting technology, named the Multi-dimensional Optimal Order Detection (MOOD), has been proposed and tested for the Euler system [5, 6, 8]. An extension version has been proposed for the non-conservative shallow water equations where a sixth-order scheme was tested on two-dimensional unstructured meshes [7]. We here tackle the question of comparing the efficiency of the MOOD and MUSCL second-order methods. The two techniques are fundamentally different since the MUSCL is based on *a priori* criteria, whereas the MOOD uses *a posteriori* detectors to prevent the solution from oscillating in the vicinity of discontinuities.
This work proposes a comparison study between the two methods for the simple one-dimensional case in order to assess their accuracy and shock capturing capacity, as well as dry/wet interfaces location. After developing the key ingredients of the discretization, we introduce the MUSCL and MOOD methods and highlight their differences. Numerical tests are then carried out to draw the comparisons using four relevant simulations: the lake at rest to check the C-property, a regular case for the accuracy, a discontinuous case for the shock capturing, and finally a set of two dry/wet tests to evaluate both methods in this specific but important configuration (flooding, dam break or tsunami).

2 SECOND-ORDER FINITE VOLUME SCHEME

The classical shallow water system with varying bathymetry writes

$$\begin{aligned} \partial_t h + \partial_x(hu) &= 0, \\ \partial_t(hu) + \partial_x\left(hu^2 + \frac{g}{2}h^2\right) &= -gh\partial_x b, \end{aligned}$$

where h denotes the water height, u the velocity, b the bathymetry, $g = 9.81$ the gravity acceleration, and $\eta = h + b$ the free surface. Vector $U = (h, hu, b)$ represents the conservative quantities.

2.1 Discretization

Domain $\Omega = [0, L]$ is decomposed into non-overlapping cells $c_i = [x_{i-1/2}, x_{i+1/2}]$ with centroid x_i, $i = 1, \cdots, I$. For a final time T, $0 = t^0 < t^1 < \cdots < t^n < \cdots < t^N = T$ is a regular subdivision with time step $\Delta t = \frac{T}{N}$. We denote by $\Delta x_i = |c_i|$ the length of the cell, while α_i^n represents an approximation of the mean value over cell c_i for function α

($\alpha = h, \eta, hu, b$) at time t^n. We recall that for regular functions (say C^2) over the cell c_i, the point-wise value at x_i is a second-order approximation of the mean value. In the same way, $\alpha^n_{i+1/2,L}$ and $\alpha^n_{i+1/2,R}$ represent approximations on the left and right side of $x_{i+1/2}$.

2.2 Hydrostatic reconstruction

We recall the hydrostatic reconstruction introduced by Audusse *et al.* [1]. We denote by $b^n_{i+1/2} = \max(b^n_{i+1/2,L}, b^n_{i+1/2,R})$ and set

$$h^{*,n}_{i+1/2,L} = \max(0, h^n_{i+1/2,L} - b^n_{i+1/2} + b^n_{i+1/2,L}), \quad \eta^{*,n}_{i+1/2,L} = h^{*,n}_{i+1/2,L} + b^n_{i+1/2},$$
$$h^{*,n}_{i+1/2,R} = \max(0, h^n_{i+1/2,R} - b^n_{i+1/2} + b^n_{i+1/2,R}), \quad \eta^{*,n}_{i+1/2,R} = h^{*,n}_{i+1/2,R} + b^n_{i+1/2}.$$

For the sake of consistency, we also set $u^{*,n}_{i+1/2,L} = u^n_{i+1/2,L}$ and $u^{*,n}_{i+1/2,R} = u^n_{i+1/2,R}$.

2.3 Generic second-order scheme

We use the Audusse *et al.* methodology [1, 9], where the following scheme has been proposed

$$U^{n+1}_i = U^n_i - \frac{\Delta t}{\Delta x_i}\left[\mathcal{F}^n_{i+1/2} + \varepsilon^n_{i+1/2,L} - F^n_{i-1/2} - \varepsilon^n_{i-1/2,R}\right] + \Delta t \mathcal{S}^n_i,$$

with $\mathcal{F}^n_{i-1/2} = \mathbb{F}(U^{*,n}_{i-1/2,L}, U^{*,n}_{i-1/2,R})$ the numerical flux for the conservative contribution (Rusanov or HLL for example [12]) with

$$U^{*,n}_{i-1/2,L} = \begin{pmatrix} h^{*,n}_{i-1/2,L} \\ h^{*,n}_{i-1/2,L} u^{*,n}_{i-1/2,L} \\ b^n_{i-1/2} \end{pmatrix}, \quad U^{*,n}_{i-1/2,R} = \begin{pmatrix} h^{*,n}_{i-1/2,R} \\ h^{*,n}_{i-1/2,R} u^{*,n}_{i-1/2,R} \\ b^n_{i-1/2} \end{pmatrix}.$$

We introduce the non-conservative numerical flux to deal with the discontinuous part of the non-conservative source term

$$\varepsilon^n_{i+1/2,L} = \frac{g}{2}\left[(h^{*,n}_{i+1/2,L})^2 - (h^n_{i+1/2,L})^2\right], \quad \varepsilon^n_{i-1/2,R} = \frac{g}{2}\left[(h^{*,n}_{i-1/2,R})^2 - (h^n_{i-1/2,R})^2\right],$$

while the discretization of the regular part of the non-conservative source term writes

$$\mathcal{S}^n_i = -g\frac{h^n_{i+1/2,L} + h^n_{i-1/2,R}}{2} \times \frac{b^n_{i+1/2,L} - b^n_{i-1/2,R}}{\Delta x_i}.$$

3 MUSCL versus MOOD

To provide a second-order scheme, local linear reconstructions are required, and therefore we compute slopes to provide an approximation of the first derivatives (see [4] for an overview of the MUSCL method). For any function $\alpha = h, \eta, hu, b$, we define the slopes

$$p^n_{i-1/2}(\alpha) = 2\frac{\alpha^n_i - \alpha^n_{i-1}}{\Delta x_{i-1} + \Delta x_i}, \quad p^n_{i+1/2}(\alpha) = 2\frac{\alpha^n_{i+1} - \alpha^n_i}{\Delta x_i + \Delta x_{i+1}},$$
$$p^n_i(\alpha) = 2\frac{\alpha^n_{i+1} - \alpha^n_{i-1}}{\Delta x_{i-1} + 2\Delta x_i + \Delta x_{i+1}}.$$

The first-order scheme corresponds to take $\alpha^n_{i+1/2,L} = \alpha^n_{i-1/2,R} = \alpha^n_i$, that is $p^n(\alpha) = 0$. Notice that for that case, we have $\mathcal{S}^n_i = 0$ and the contribution of bathymetry variations is concentrated on the interfaces. It is well-known that a non-limited linear reconstruction will give rise to oscillations in the vicinity of a discontinuity due to the Gibbs phenomenon and non-linear limiting procedures have to be implemented to locally reduce the accuracy and preserve the monotonicity. Based on linear reconstructions, the traditional MUSCL approach consists in reducing the slopes such that some stability criterion is achieved. Thus, such a method is *a priori* since the corrections are made before updating the solution. On the contrary, the MOOD method assumes that the solution is smooth enough. A candidate solution is computed without altering the slopes and then, based on the candidate solution, corrections of the slopes are provided to satisfy some stability criterion. The *a posteriori* method has the advantage to perform corrections only for problematic cells and therefore this technique is less intrusive and provides better accuracy.

3.1 MUSCL method

The MUSCL second-order scheme corresponds to define the reconstructed values on the left and right side of the interfaces by

$$\alpha^n_{i+1/2,L} = \alpha^n_i + q^n_i(\alpha)\frac{\Delta x_i}{2}, \quad \alpha^n_{i-1/2,R} = \alpha^n_i - q^n_i(\alpha)\frac{\Delta x_i}{2},$$

where the limited slope

$$q^n_i(\alpha) = \phi\left(p^n_{i-1/2}(\alpha), p^n_{i+1/2}(\alpha)\right)$$

is computed using a limiter function ϕ such as the min-mod, the van-Alabada or the van-Leer limiters. An important point is that the reconstruction cannot be performed with h, η and b at the same time for compatibility reasons. It has been proved that the good choice is to carry out the MUSCL procedure on h and η, and then deduce the values for b on the interfaces (this is the reason why b depends on time) setting

$$b^n_{i+1/2,L} = \eta^n_{i+1/2,L} - h^n_{i+1/2,L}, \quad b^n_{i-1/2,R} = \eta^n_{i-1/2,R} - h^n_{i-1/2,R}.$$

Notice that a second-order method in space also requires a second-order method in time to be effective. The usual TVD-RK2 (Heun method) is employed to guarantee a global second-order method for smooth solutions.

3.2 MOOD method

We give here a short introduction to the MOOD method, but a detailed description is given in [5, 6, 8, 7, 2]. The Cell Polynomial Degree (CPD) map corresponds to a vector associated to the cells which indicates the degree of the polynomial reconstruction, while the Edge Polynomial Degree (EPD) is a vector associated to the edges indicating the degree of the polynomial used to evaluate the reconstruction on both sides of the edges for the flux and source term computation. In practice, we take $\mathrm{EPD}(i + 1/2) =$

$\min(\text{CPD}(i), \text{CPD}(i+1))$. In our specific case, a cell c_i may have a $\text{CPD}(i) = 1$ if we use the slope (second-order approximation) or $\text{CPD}(i) = 0$ if the slope is null (first-order approximation).
The MOOD method is based on the following loop. Assume that we known an approximation $U_h^n = (U_i^n)_{i=1,\cdots,I}$ at time t^n and initialise the CPD to 1, *i.e.* we use a second-order approximation for each cell.

1. We build a candidate solution $U_h^\star$ based on the CPD map. In practice, we use the reconstruction indicated by the corresponding EPD map to compute the reconstructed values used to evaluate the numerical fluxes and the source term.

2. We look at each value $U_i^\star$ of the candidate solution to check if it satisfies a set of conditions (or detectors).

3. If all the cells are valid, then the candidate solution turns out to be the approximation at time t^{n+1}, *i.e.* $U_h^{n+1} = U_h^\star$. Otherwise, we modify the CPD map reducing the polynomial degree from 1 to 0 for the problematic cells and go back to step 1.

The MOOD method assumes that the first-order scheme (the CPD map is zero everywhere) fulfils the set of conditions. Hence, in the worst case, the scheme becomes a first-order one.

3.2.1 Basic detectors

Several detectors may be defined to determine whether a cell is eligible or not as proposed in [7]. The main point is to detect if the candidate solution is physically admissible and to prevent the appearance of oscillations characterised by creation of local extrema.

Physical Admissible Detector (PAD) The candidate solution satisfies the PAD condition on cell c_i if $h_i^\star \geq 0$. Such a condition is crucial since negative water height values are non-physical.

Maximum Principle Detector (MPD) The candidate solution satisfies the MPD condition on cell c_i if

$$\min(h_{i-1}^n, h_i^n, h_{i+1}^n) \leq h_i^\star \leq \max(h_{i-1}^n, h_i^n, h_{i+1}^n),$$

which implies that the candidate value remains between the local minimum and local maximum at time t^n. Such condition enables to detect potential oscillation since the Gibbs phenomenon induces the creation of local extrema.

Extrema Detector (ED) In the case where the solution does not depend on time, the MPD condition does not make sense and therefore it is useful to consider the new following criterion

$$\min(h^\star_{i-1}, h^\star_{i+1}) \leq h^\star_i \leq \max(h^\star_{i-1}, h^\star_{i+1}),$$

which allows to detect the extrema of the discrete candidate solution.

3.2.2 Relaxation detectors

Extrema may derive from local oscillations associated to the Gibbs phenomenon, but may also be smooth extrema corresponding to real ones. Hence, we have to distinguish these two situations in order to set the CPD $= 0$ for the oscillation case, whereas in the other case we preserve the CPD $= 1$ to provide a second-order of approximation. To this end, we introduce a new tool. For any function $\alpha = h, \eta, hu$, we set

$$C_i(\alpha) = \frac{\alpha_{i+1} + \alpha_{i-1} - 2\alpha_i}{(\Delta x)^2},\ i = 2, \ldots, I-1, \quad \text{and} \quad C_1(\alpha) = C_2(\alpha),\ C_I(\alpha) = C_{I-1}(\alpha),$$

where for the sake of simplicity we assume $\Delta x_i = \Delta x$, and compute the following local curvature indicators

$$\chi_{m,i} = \min(C_{i-1}, C_i, C_{i+1}), \quad \chi_{M,i} = \max(C_{i-1}, C_i, C_{i+1}),$$

for $i = 2, \ldots, I-1$, where we omit the function α for the sake of simplicity. Notice that one can have $|\chi_{m,i}| > |\chi_{M,i}|$. We then define the following relaxation limiters.

Small Curvature Detector (SCD) or Plateau Detector Let ε_C be a given tolerance parameter. Then, CPD$(i) = 1$ if

$$\max(|\chi_{m,i}|, |\chi_{M,i}|) \leq \varepsilon_C.$$

Such condition means that the curvature is so small that the numerical solution is locally linear and therefore the reconstruction should not be limited.

Local Oscillation Detector (LOD) We must enforce CPD$(i) = 0$ if one has

$$\chi_{m,i}\chi_{M,i} \leq 0.$$

This condition detects a local oscillation due to the variation of the curvatures sign.

Smoothness Detector(SD) Let ε_S be a given tolerance parameter. The numerical solution is considered locally smooth if

$$1 \geq \frac{\min(|\chi_{m,i}|, |\chi_{M,i}|)}{\max(|\chi_{m,i}|, |\chi_{M,i}|)} \geq 1 - \varepsilon_S.$$

If that is the case we set CPD$(i) = 1$. This detector determines if the minimum and the maximum curvatures are close enough with respect to the threshold parameter and the numerical solution is considered locally smooth.

3.2.3 Condition for solution eligibility

Since the MOOD procedure can involve up to six detectors, we now detail how the detectors are linked one to each to other and are used to determine if the CPD is 0 (non-admissible candidate solution) or 1 (admissible). The detector chain is given in Figure 1 where for each cell, the algorithm detection provides the new value of the CPD.

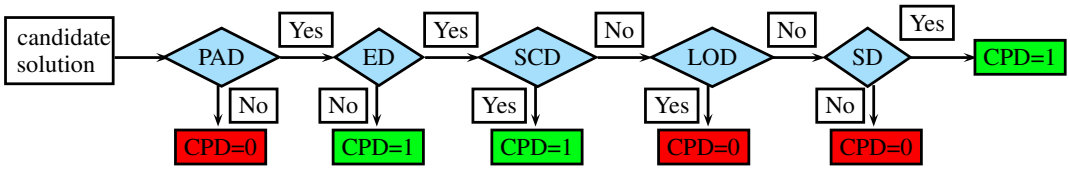

Figure 1: The chain detectors algorithm for the MOOD method.

4 NUMERICAL SIMULATIONS

Numerical tests are carried out to assess the performance of the two schemes. The time step Δt is controlled by the CFL condition reduced by a factor 0.4 with respect to the maximum admissible time step of the first-order scheme. All meshes are constituted by cells having equal length $\Delta x = L/I$. The HLL flux scheme is used in all numerical simulations since it is less diffusive than the Rusanov one. For the MUSCL method the limiter procedure is applied to h, η, and $q = hu$, whereas for the MOOD method only the water height h is considered in the detector procedures. In the MOOD case the relaxation parameters used within the detector scheme are $\varepsilon_C = \delta^3$ and $\varepsilon_S = 0.5$, where $\delta = \Delta x/L = 1/I$ (see [7]). Finally, when dry/wet interfaces are present, after each integration step we perform a clipping where we set the water height equal to zero if $h < 10^{-6}$.
To assess the convergence, we introduce the L^1- and L^∞-errors as

$$L^1\text{-error: } \sum_{i=1}^{I} |\alpha_i^N - \alpha_i^{ex}|/I \quad \text{and} \quad L^\infty\text{-error: } \max_i |\alpha_i^N - \alpha_i^{ex}|,$$

where (α_i^{ex}) and (α_i^N) are respectively the exact and the approximated mean values on cell c_i at the final time $t^N = T$.

4.1 Lake at rest

Lake at rest simulation is the first sanity check experience to test the C-property, *i.e.* the preservation of the steady-state situation with null velocity [3]. On domain $[0, 1]$, we assume that the fluid is initially at rest, *i.e.* $q = u = 0$, while the bathymetry b and its first derivative present some discontinuities and the total height $\eta = \max(2, b)$ has various

dry/wet interfaces (see Figure 2). We consider successive meshes with 50, 100, and 200 cells, and compute the solution until the final time $T = 1$ corresponding to 554, 1108 and 2215 time steps, respectively. In the simulations, reflection conditions are prescribed at the boundary.

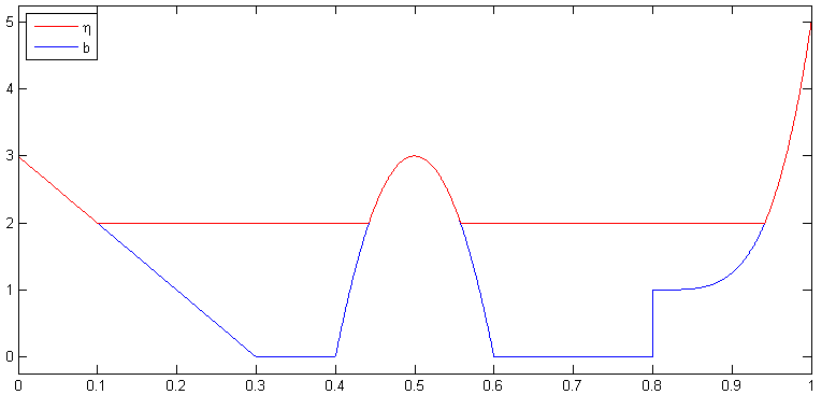

Figure 2: Bathymetry function and total height for the lake at rest.

After performing all the numerical tests, we report that the L^1- and L^∞-errors for η, h, q and u stand below 10^{-15} and 10^{-14}, respectively. Since the calculations are performed in double precision, we conclude that both MUSCL and MOOD implementations satisfy the C-property.

4.2 Smooth solution

We now turn to the regular case where we assess the schemes accuracy. We want to evaluate the impact of the limiting/detecting procedures when an optimal second-order approximation should be achieved. We intend to draw some comparisons between the MUSCL and MOOD schemes and determine which scheme provides the best performance. For this purpose, we consider a steady-state supercritical flow and evaluate the approximation which intends to preserve the stationary regime. The flow considered has the upstream boundary located at $x = 0$ and the downstream one at $x = L$ (we consider a channel with length $L = 10$). The stationary solution is given by

$$q(x) = q_0, \quad \frac{q_0^2}{2gh^2(x)} + h(x) + b(x) = \frac{q_0^2}{2gh^2(0)} + h(0) + b(0).$$

where we take $q_0 = 13.29$, and $h(0) = \eta(0) - b(0)$ with $\eta(0) = 2$ (see e.g. [13]). The bathymetry function is the exponential bump $b(x) = 0.2\exp(-5(x-4)^2))$ plotted in Figure 3 together with the free surface.

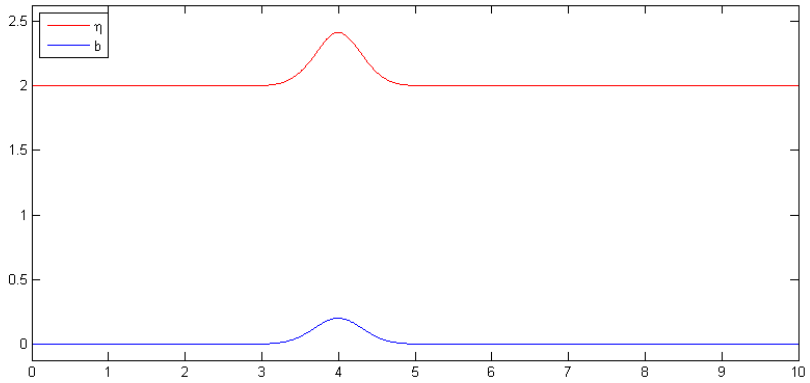

Figure 3: Bathymetry function and free surface for the supercritical stationary flow.

Given the nature of the flow - supercritical with a Froude number larger than 1.25 - Dirichlet boundary conditions are prescribed at $x = 0$, whereas transmission conditions hold at the downstream boundary. The initial condition is the steady-state solution and the numerical simulations are carried out until $t = 10$ for meshes with 100, 200, 400, 800 and 1600 cells, involving up to 44298 time steps.
We test the MOOD method with two different detectors chains: the first one omits the Small Curvature Detector (SCD or plateau detector), whereas the second one uses the full set of detectors as presented in Figure 1. The goal to skip the SCD is to draw a comparison with the MUSCL scheme in similar conditions, since the latter method cannot distinguish between very small variations deriving from the real number truncation and the non-physical oscillations. Notice that the proposed simulation involves a solution which is essentially flat far away from the bump, hence the SCD deactivation could be decisive. In that particular simulation, the MUSCL limiter only involves the conservative variable h since it provides the best results.

Table 1: Total height and velocity L^1- and L^∞-errors and convergence order for the supercritical case: MUSCL scheme.

Nb of Cells	η				u			
	err_1		err_∞		err_1		err_∞	
100	2.44e-03	—	4.76e-02	—	5.40e-03	—	7.91e-02	—
200	5.20e-04	2.2	2.05e-02	1.2	1.12e-03	2.3	3.38e-02	1.2
400	1.12e-04	2.2	5.77e-03	1.8	2.38e-04	2.2	9.52e-03	1.8
800	2.30e-05	2.3	1.47e-03	2.0	4.89e-05	2.3	2.43e-03	2.0
1600	5.43e-06	2.1	3.73e-04	2.0	1.16e-05	2.1	6.15e-04	2.0

Tables 1, 2 and 3 provide the L^1- and L^∞-errors and convergence order for the MUSCL

Table 2: Total height and velocity L^1- and L^∞-errors and convergence order for the supercritical case: MOOD scheme without SCD. The percentage of cells having maximum CPD at $t = T$ is also shown.

Nb of Cells	η				u				Cells with CPD = 1
	err_1		err_∞		err_1		err_∞		
100	1.81e-03	—	2.93e-02	—	5.30e-03	—	8.33e-02	—	73%
200	7.02e-05	4.7	1.22e-03	4.6	1.74e-04	4.9	4.23e-03	4.3	91%
400	8.43e-06	3.1	1.29e-04	3.2	2.10e-05	3.1	2.73e-04	4.0	88%
800	1.45e-06	2.5	2.21e-05	2.5	3.81e-06	2.5	5.12e-05	2.4	100%
1600	2.86e-07	2.3	4.26e-06	2.4	7.84e-07	2.3	1.07e-05	2.3	100%

Table 3: Total height and velocity L^1- and L^∞-errors and convergence order for the supercritical case: full detectors chain. The percentage of cells having maximum CPD at $t = T$ is also shown.

Nb of Cells	η				u				Cells with CPD = 1
	err_1		err_∞		err_1		err_∞		
100	1.91e-03	—	3.15e-02	—	5.06e-03	—	6.88e-02	—	91%
200	5.23e-05	5.2	8.19e-04	5.3	1.24e-04	5.4	1.61e-03	5.4	100%
400	8.49e-06	2.6	1.29e-04	2.7	2.13e-05	2.5	2.73e-04	2.6	100%
800	1.45e-06	2.5	2.21e-05	2.5	3.81e-06	2.5	5.12e-05	2.4	100%
1600	2.86e-07	2.3	4.26e-06	2.4	7.84e-07	2.3	1.07e-05	2.3	100%

scheme, the MOOD scheme without the SCD detector, the MOOD scheme with the full detectors chain, respectively, while we report in the two last tables the percentage of cells that have CPD = 1 at $t = T$ for the MOOD method.
Clearly the MOOD method provides smaller errors and the better convergence order of accuracy. We note that the deactivation of the SCD does not affect the global error since we are dealing with a plateau, *i.e.* the first-order and the second-order schemes provide the same results in that zone. The top of the bump is relaxed by the MOOD Smooth Detector providing the optimal CPD, *i.e.* the approximation is a second-order one in the vicinity of the extremum, whereas the MUSCL strongly cuts the slope leading to significant negative impact on the accuracy.

4.3 Dam break on a wet bed

Having tackled the smooth solution case, we now consider the dam break problem since it involves a shock and therefore comparisons between the two methods can be performed following two criteria: the presence (or not) of oscillations and the number of intermediate cells in the shock. For that, we consider the domain $[0, 50]$ and assume the initial configuration: $\eta(x) = 5$ for $0 \leq x \leq 25$, $\eta(x) = 1$ for $25 < x \leq 50$, $u(x) = 0$ on the whole domain and the bathymetry is flat with $b(x) = 0$. The simulations are carried out for a 100 cells mesh using reflection boundary conditions, and we evaluate the approximation at the final simulation time $T = 3$.

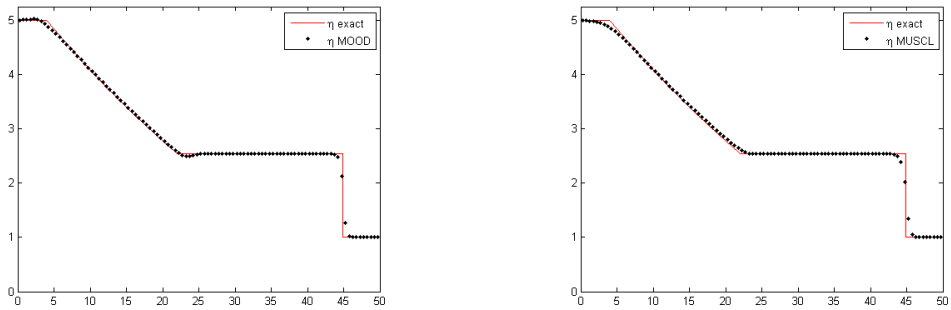

Figure 4: Exact and approximated total height for the dam break case for the MOOD (left) and MUSCL (right) methods with 100 cells.

Figures 4 and 5 present the free surface and the velocity for the MOOD (left) and the MUSCL (right) methods. In both cases, no oscillations are reported and we observe that there are 3 cells in the η-shock for the MUSCL case, whereas the MOOD technique manages to capture the shock within only 2 cells. In the MOOD case, we notice a small numerical artefact at the end of the rarefaction ($x = 22$) since the transition presents a discontinuity of the derivative whereas the CPD map remains equal to one in the vicinity of the transition. The CPD map should be zeroed at that point and the detector fails to see such discontinuity. A new detector should be provided to correctly perform the treatment of such a transition.

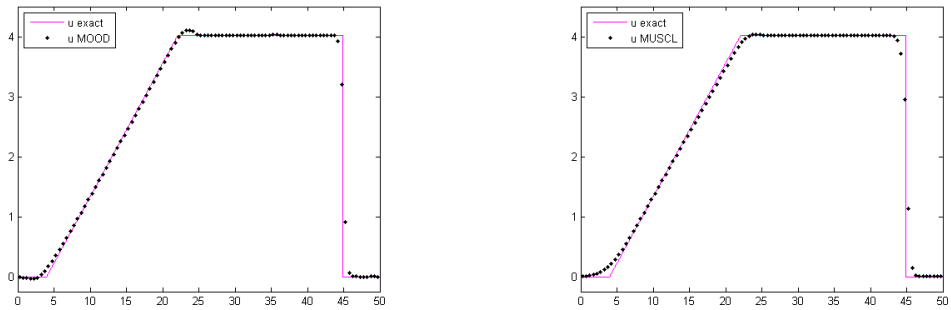

Figure 5: Exact and approximated velocity for the dam break case for the MOOD (left) and MUSCL (right) methods with 100 cells.

When dealing with rough solutions, the convergence order of the errors is not relevant (almost equal to one in our case), but the multiplicative constant is of crucial importance. Indeed, if one assumes a convergence order of the form $\text{err} = C(\Delta x)^{\beta}$, for rough solutions one has $\beta = 1$, but the choice of the scheme may affect the value of C. In Figure 6

we display the L^1-norm convergence curves for the total height and the velocity and observe that the corresponding multiplicative constants are lower for the MOOD method ($C_\eta = 10^{-1.43}$, $C_u = 10^{-1.14}$) with respect to the MUSCL one ($C_\eta = 10^{-1.26}$, $C_u = 10^{-0.97}$).

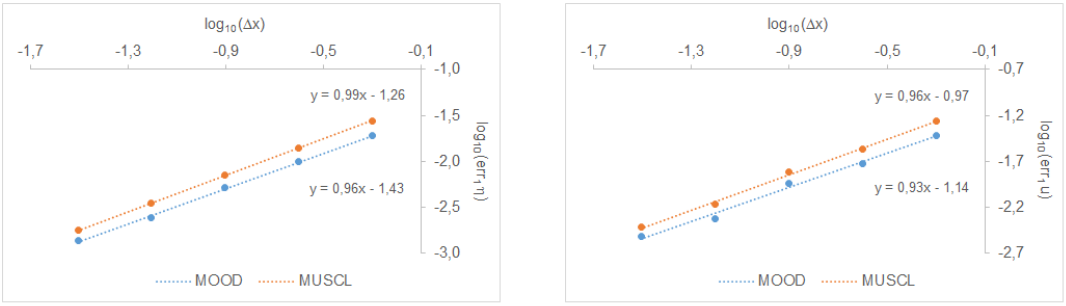

Figure 6: Comparison of the total height (left) and velocity (right) L^1-errors for the dam break case for the MOOD and MUSCL methods.

4.4 Dry/wet simulation

Dry/wet interface approximation is a fundamental issue to be addressed when dealing with coastal problems or flooding. The capacity to provide good approximations of the velocity close to the interface is crucial for the applications since the impact of waves or flooding is deeply linked to the kinetic energy or the friction force associated to the flow velocity. We propose here two representative test cases, namely a smooth bathymetry situation which corresponds to a coastal problem and a discontinuous bathymetry representing a wave impact on a wall.

4.4.1 Smooth bathymetry

In this simulation we consider the domain $[0, 50]$ and choose a smooth bathymetry function given by $b(x) = 0$ for $0 \leq x \leq 20$, $b(x) = 0.15(x - 20)$ for $20 < x \leq 50$. The initial configuration concerning the total height is $\eta(x) = 5$ for $0 \leq x \leq 25$, $\eta(x) = b(x)$ for $25 < x \leq 50$. The initial velocity, the boundary conditions and the number of cells are the same considered in the previous test. The final simulation time is $T = 1.5$.
We plot in Figures 7 and 8, respectively, the free surface and the velocity, for the first-order scheme with 10 000 cells as a reference solution, as well as for the approximations with the MOOD and MUSCL methods. We report that the MOOD method has a small over-estimated water height close to the dry/wet interface, but the velocity is very well approximated. On the contrary, the MUSCL method provides smoother water height

close to the interface but the velocity is over-estimated. The figures show that the MOOD technique manages to correctly handle the interface.

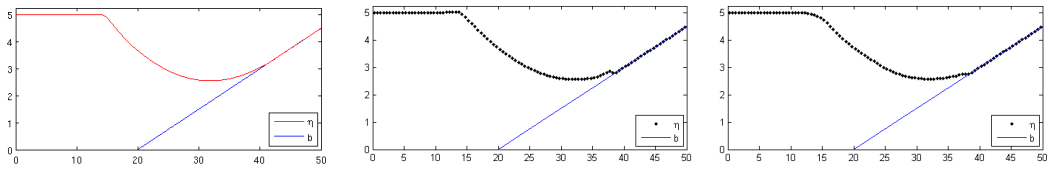

Figure 7: Total height with the first-order (left with 10 000 cells), the MOOD (middle) and MUSCL (right) method for the dry/wet case with smooth bathymetry (100 cells).

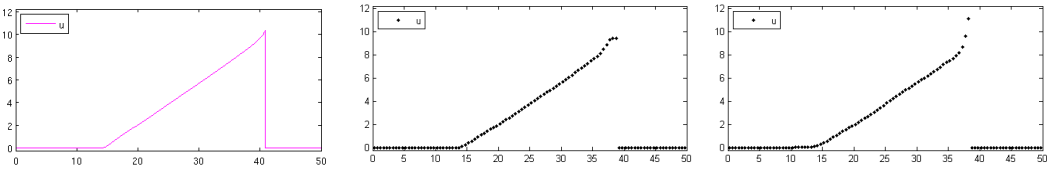

Figure 8: Velocity with the first-order (left with 10 000 cells), the MOOD (middle) and MUSCL (right) method for the dry/wet case with smooth bathymetry (100 cells).

4.4.2 Discontinuous bathymetry

In this simulation we consider the domain $[0, 50]$ and choose a discontinuous bathymetry function given by $b(x) = 0$ for $0 \leq x \leq 35$, $b(x) = 3 + 0.125(x - 35)$ for $35 < x \leq 50$. The initial configuration concerning the total height and velocity, as well as the boundary conditions and the number of cells are the same considered in dam break test. The final simulation time is $T = 2.75$. Numerical simulations are carried out where the first-order case is calculated with 10 000 cells to provide a reference solution. Figures 9 and 10 present, respectively, the free surface and the velocity for the first-order scheme and the approximations with the MOOD and MUSCL methods. We report that the MOOD method provides a slightly sharper shock in the transition with respect to the MUSCL method. Moreover, the velocity is well approximated with the MOOD case and over-estimated with the MUSCL technique. As in the smooth case, a small over-estimation of the water height occurs with the MOOD method.

5 CONCLUSIONS

We propose in the present work a comparison between the MOOD and the MUSCL methods to achieve second-order approximation of the shallow water equations. We report

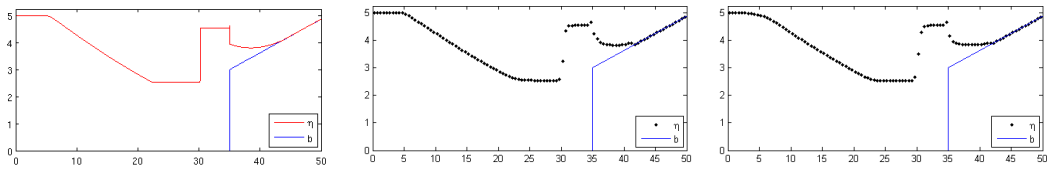

Figure 9: Total height with the first-order (left with 10 000 cells), the MOOD (middle) and MUSCL (right) method for the dry/wet case with discontinuous bathymetry (100 cells).

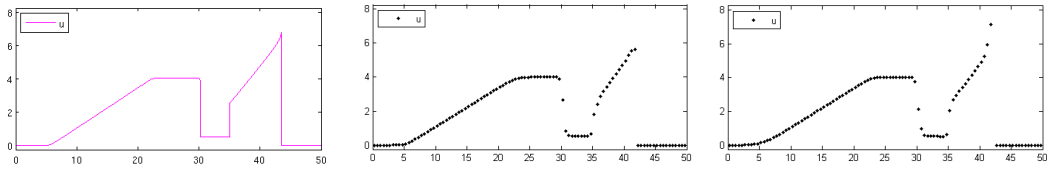

Figure 10: Velocity with the first-order (left with 10 000 cells), the MOOD (middle) and MUSCL (right) method for the dry/wet case with discontinuous bathymetry (100 cells).

that the MOOD method is less diffusive regarding to the MUSCL one and manages to treat very well the non-conservative term. Critical situations such as dry/wet interface with smooth or discontinuous bathymetry are also well treated by the MOOD methodology. Nevertheless, new detectors have to be proposed to overcome the small over-estimation of the water height in the case of smooth ramps.

ACKNOWLEDGEMENTS

This research was financed by FEDER Funds through Programa Operational Fatores de Competitividade — COMPETE and by Portuguese Funds FCT — Fundação para a Ciência e a Tecnologia, within the Projects PEst-C/MAT/UI0013/2014, PTDC/MAT/121185/2010 and FCT-ANR/MAT-NAN/0122/2012.

REFERENCES

[1] Audusse, E., Bouchut, F., Bristeau, M. O., Klein, R., Perthame, B., "A fast and stable well-balanced scheme with hydrostatic reconstruction for shallow water flows", *SIAM J. Sci. Comput.* Vol. **25**, pp. 2050-2065, 2004.

[2] Berthon, C., Desveaux, V., "An entropy preserving MOOD scheme for the Euler equations", *Int. J. finite volumes* Vol. **11**, pp. 1-39, 2014.

[3] Bermúdez, A., Vázquez , M. E., "Upwind methods for hyperbolic conservation laws with source terms", *Computers & Fluids* **24**, pp. 1049-1071, 1994.

[4] Buffard, T. , Clain, S., "Monoslope and multislope MUSCL methods for unstructured meshes", *J. Comput. Phys.* Vol. **229**, pp. 3745-3776, 2010.

[5] Clain, S., Diot, S., Loubère, R., "A high-order finite volume method for hyperbolic systems: Multi-dimensional Optimal Order Detection (MOOD)", *J. Comput. Phys.* Vol. **230(10)**, pp. 4028-4050, 2011.

[6] Diot, S., Clain, S., Loubère, R., "Improved Detection criteria for the Multi-dimensional Optimal Order Detection (MOOD) on unstructured meshes with very high-order polynomials", *Comput. & Fluids* Vol. **64**,pp. 43-63, 2012.

[7] Clain, S., Figueiredo, J., "The MOOD method for the non-conservative shallow water system", preprint HAL hal-01077557 (2014), submitted.

[8] Diot, S., Loubère, R., Clain, S., "The MOOD method in the three-dimensional case: Very high-order finite volume method for hyperbolic systems", *Int. J. Numer. Meth. Fluids* Vol. **73**, pp. 362-392, 2013.

[9] Duran, A., Liang, Q., Marche, F., "On the well-balanced numerical discretization of shallow water equations on unstructured meshes", *J. compt. phys.* Vol. **235**, pp. 565-586, 2013.

[10] Noelle, S., Pankratz, N., Puppo, G., Natvig, J. R., "Well-balanced inite volume schemes of arbitrary order of accuracy for shallow water flows", *J. Comput. Phys.* Vol **213**, pp. 474-499, 2006.

[11] Noelle, S., Xing, Y., Shu, C.-W., "High-order well-balanced finite volume WENO schemes for shallow water equations with moving water", *J. Comput. Phys.* Vol **226**, pp. 29-58, 2007.

[12] Toro, E. F., *Riemann Solvers and Numerical Methods for Fluid Dynamics*, 3^{rd} revision, Springer-Verlag Berlin and Heidelberg GmbH & Co. K 2009.

[13] Delestre, O., Lucas, C., Ksinant, P.-A., Darboux, F., Laguerre, C., Vo,T.-N.-T., James, F., Cordier, S., "SWASHES: a compilation of shallow water analytic solutions for hydraulic and environmental studies", *Int. J. Numer. Meth. Fluids* Vol. **72** pp. 269-300, 2013.

[14] Wijetunge, J. J., "Numerical simulation of the 2004 indian ocean tsunami: case study of effect of sand dunes on the spatial distribution of inundation in Hambantota, Sri Lanka", *J. Appl. Fluid Mech.* Vol. **3**, pp. 125-135, 2010.

[15] Zhou, J. G., Causon, D. M., Mingham, C. G., Ingram, D. M., "Numerical solutions of the shallow water equations with discontinuous bed topography", *Int. J. Numer. Meth. Fluids* Vol. **38**, pp. 769-788, 2002.